Carrier localization in quaternary $Ga_{1-x}Mn_xAs_{1-y}P_y$ ferromagnetic semiconductor films

Sining Dong,[1,2] Logan Riney,[1] Xinyu Liu ●,[1,*] Lei Guo,[3] Ren-Kui Zheng,[3,4] Xiang Li,[1] Seul-Ki Bac,[1,5] Jacek Kossut,[6] Margaret Dobrowolska,[1] Badih Assaf,[1] and Jacek K. Furdyna ●[1]

[1]*Department of Physics, University of Notre Dame, Notre Dame, Indiana 46556, USA*
[2]*Research Institute of Superconductor Electronics, School of Electronic Science and Engineering, Nanjing University, Nanjing 210093, China*
[3]*Shanghai Institute of Ceramics, Chinese Academy of Sciences, Shanghai 200050, China*
[4]*School of Materials Science and Engineering, Jiangxi Engineering Laboratory for Advanced Functional Thin Films,*
Nanchang University, Nanchang 330031, China
[5]*Department of Physics, Korea University, Seoul 136-701, Korea*
[6]*Institute of Physics, Polish Academy of Sciences, 02-668 Warszawa, Poland*

Motivated by the fact that holes in the $Ga_{1-x}Mn_xAs$ family of ferromagnetic semiconductors play a key role in determining their ferromagnetic properties, we have measured hole concentrations in a series of three $Ga_{1-x}Mn_xAs_{1-y}P_y$ alloys grown by molecular beam epitaxy with varying amounts of phosphorus. This was carried out by Hall effect measurements, after eliminating the effect of the anomalous Hall term, and thus isolating the ordinary Hall term that directly provides the concentration of freely moving holes. Comparing these Hall effect results with total hole concentrations obtained from the number of acceptors and compensating donors as given by structural and magnetization measurements, we find that the number of itinerant holes (i.e., holes that contribute to the Hall effect) is significantly less than the total hole concentration. This indicates that a considerable fraction of the holes arising from Mn acceptors are localized. We find, furthermore, that the degree of such localization increases with the concentration of phosphorus in the $Ga_{1-x}Mn_xAs_{1-y}P_y$ alloy. Our results indicate that the Curie temperature (and, by extension, other magnetic properties) described by the Zener model in ferromagnetic semiconductors of the $Ga_{1-x}Mn_xAs$ family are determined by the itinerant holes rather than by the total hole concentration. Finally, our results also indicate that ferromagnetism in these alloys vanishes when the total hole concentration falls below a certain Mott-like threshold, suggesting that the holes (both localized and itinerant) reside in the acceptor impurity band created by the presence of Mn acceptors.

I. INTRODUCTION

The quaternary alloy $Ga_{1-x}Mn_xAs_{1-y}P_y$ is a ferromagnetic semiconductor closely related to the well-known $Ga_{1-x}Mn_xAs$ family of ferromagnetic alloys [1,2]. It is of special interest because, when grown epitaxially on GaAs, the presence of phosphorus can be used to manipulate strain in $Ga_{1-x}Mn_xAs_{1-y}P_y$ films, and thus their magnetic anisotropy [3]. As an example, at sufficiently high concentrations of phosphorus (about 10 at. %) the tensile strain in $Ga_{1-x}Mn_xAs_{1-y}P_y$ is sufficient to turn the magnetic easy axis normal to the film plane [4,5], which opens the path to a number of alternative physical effects [6,7] as well as unique spintronic applications [8–10].

Since this alloy is closely related to $Ga_{1-x}Mn_xAs$, it can be assumed that its magnetic properties depend critically on its hole concentration [11]. However, this aspect of $Ga_{1-x}Mn_xAs_{1-y}P_y$, and especially the dependence of its hole concentration on the phosphorus content of the alloy, has not been fully studied [12,13]. Generally $Ga_{1-x}Mn_xAs_{1-y}P_y$ films are viewed as behaving similarly to $Ga_{1-x}Mn_xAs$ films, but (quite apart from the ability to control strain in this alloy), there exist significant differences between $Ga_{1-x}Mn_xAs_{1-y}P_y$

and $Ga_{1-x}Mn_xAs$ that deserve attention [5,14,15]. These include a significant difference of the energy gap between the two materials, the location of the impurity band (whose role in determining ferromagnetic properties continues to be a subject of considerable debate), and additional disorder due to the presence of two anions in the $Ga_{1-x}Mn_xAs_{1-y}P_y$ system.

Motivated by these differences, in this paper we carry out a systematic study of how transport properties (and, in particular, the properties of holes) depend on the phosphorus content in $Ga_{1-x}Mn_xAs_{1-y}P_y$. Specifically, we investigate the dependence of hole concentration in a series of specimens with varying concentration of P between ∼10 and ∼20 at. %, i.e., where the presence of P is sufficiently high to have significant consequences. We will show that, in addition to measuring the hole concentration and its dependence on the phosphorus content, a number of insights into the properties of $Ga_{1-x}Mn_xAs_{1-y}P_y$ also emerge from the analysis of our transport data. The logarithm used in the paper is of base 10.

II. EXPERIMETNAL PROCEDURE

A. Specimen preparation

$Ga_{1-x}Mn_xAs_{1-y}P_y$ films with a fixed value of Mn concentration of $x = 0.06$ and with phosphorus concentrations

TABLE I. Properties of as-grown and annealed $Ga_{0.94}Mn_{0.06}As_{1-y}P_y$ films.

		0.10	0.15	0.21
P concentration y		0.10	0. 15	0.21
Sample thickness t (nm)		48.3	74.3	47.2
Lattice constant a (Å)	As grown	5.64885	5.63995	5.62696
	Annealed	5.64217	5.63459	5.61860
Curie temperature (K)	As grown	59	48	40
	Annealed	96	80	87
Saturation magnetization at 5 K (emu/cm^3)	As grown	29.0	28.0	23.9
	Annealed	38.3	35.3	40.7

$y = 0.10, 0.15$, and 0.21 were grown on semi-insulating GaAs (100) substrates using low-temperature molecular beam epitaxy (MBE). The pieces of films were then annealed at $270\,°C$ for 1 h in nitrogen flux to optimize uniformity and magnetic properties of the samples. Mn content x was determined by high-resolution x-ray diffraction (HRXRD) carried out on a control $Ga_{1-x}Mn_xAs$ sample grown with identical Mn flux settings as the $Ga_{1-x}Mn_xAs_{1-y}P_y$ films used in this study. HRXRD was then used on the $Ga_{1-x}Mn_xAs_{1-y}P_y$ films to determine their crystal quality, thicknesses, and P concentrations. The Curie temperatures and saturation magnetizations of the specimens were measured using a superconducting quantum interference device (SQUID) magnetometer, and have been published in an earlier paper [5]. For electrical transport measurements, Hall bars were fabricated by photolithography with the long dimension (the current direction) along the [110] orientation of the GaAs substrate, and transport measurements were then performed at a series of temperatures in a physical property measurement system (PPMS) with a maximum field of 12.0 T. Table I summarizes the phosphorus concentrations, thicknesses, lattice constants, saturation magnetizations, and Curie temperatures of all $Ga_{1-x}Mn_xAs_{1-y}P_y$ films used in this study.

B. Measurement of free hole concentration

To measure the free (i.e., itinerant) hole concentrations in our $Ga_{1-x}Mn_xAs_{1-y}P_y$ samples we have followed the procedure of Hall and resistivity measurements used by Shen *et al.* [16]. Specifically, we measured the anomalous Hall effect (AHE) with magnetic field $\boldsymbol{B}$ applied normal to the film plane. As is well known, in ferromagnetic systems the Hall resistivity is described as a sum of two terms [17],

$$\rho_{xy} = R_0 B + R_s M, \tag{1}$$

where B is the applied field, R_0 is the ordinary Hall coefficient $R_0 = 1/pe$, M is the component of magnetization $\boldsymbol{M}$ normal to the sample plane, and R_s is the anomalous Hall coefficient. While the presence of the $R_s M$ term overshadows the standard free-carrier contribution to ρ_{xy} at typical laboratory fields, we can extract the standard Hall contribution by following the procedure developed by Shen *et al.* [16], from which the concentration p of itinerant holes can be directly obtained. (We use the term "itinerant" intentionally, since it will be seen that a fraction of the holes are localized, and thus do not contribute to R_0.)

As an illustration, in Fig. 1, we show magnetotransport data for the annealed sample $Ga_{0.94}Mn_{0.06}As_{0.85}P_{0.15}$ taken at $T = 15$ K. Results obtained on the other samples are very similar. As shown in Fig. 1(a), the Hall resistivity ρ_{xy} becomes saturated at ~ 0.02 T, and remains nearly constant throughout our field range, up to 12.0 T. Thus, the observed Hall resistivity is mainly determined by the anomalous Hall term proportional to the saturation magnetization M_s. In the inset of Fig. 1 we show the weak but clearly measurable field dependence of ρ_{xy}, that reflects the combination of the ordinary and the anomalous Hall contributions discussed later in the paper. Figure 1(b) illustrates the negative magnetoresistance observed on all six samples at low temperature. In the high-field region the resistance decreases with increasing field at a
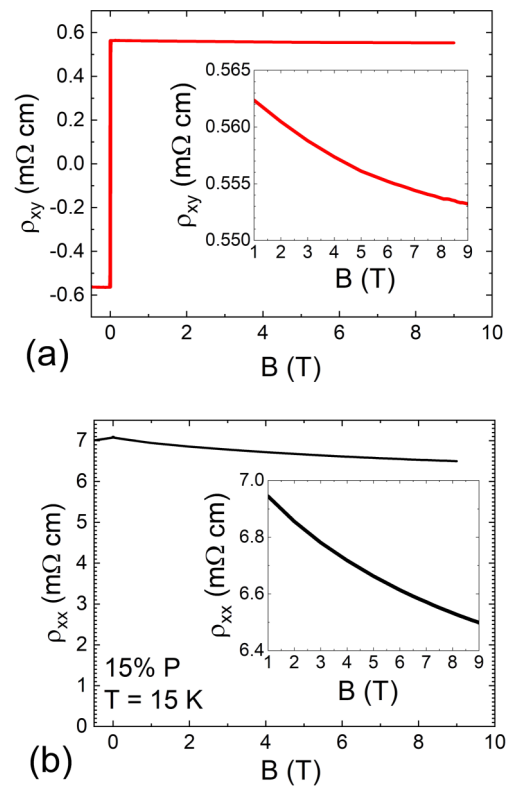

FIG. 1. (a) Hall resistivity ρ_{xy}, and (b) longitudinal resistivity ρ_{xx} as a function of field for $Ga_{0.94}Mn_{0.06}As_{0.85}P_{0.15}$ at $T = 15$ K. Field $\boldsymbol{B}$ is applied normal to the sample plane, i.e., along its easy axis. Remaining samples display very similar behavior. Insets: ρ_{xy} and ρ_{xx} shown on expanded scale.

much slower rate, but does not saturate up to 12.0 T, as seen in the inset.

C. Analysis of experimental results

As has been shown in Ref. [16], the value of the ordinary Hall term R_0B (which determines the concentration of itinerant holes) can be isolated by simultaneously measuring ρ_{xy} and ρ_{xx}, and by assuming $R_s = c\rho_{xx}^n$, where c is a constant and n is the scaling factor for the material of interest. We then have

$$\rho_{xy} = R_0B + R_SM = R_0B + c\rho_{xx}^n M. \quad (2)$$

We can determine c and n by measuring ρ_{xy} and ρ_{xx} at several temperatures, sufficiently low so that saturation magnetization M_s remains constant as the field is swept. It is also reasonable to assume that n is the same in this narrow temperature range. Rewriting Eq. (2) as $\rho_{xy} - R_0B = c\rho_{xx}^n M$ and taking the logarithm of both sides, we have

$$\log(\rho_{xy} - R_0B) = \log(cM) + n\log(\rho_{xx}). \quad (3)$$

Since $\rho_{xy} \gg R_0B$, we can write

$$\rho_{xy} - R_0B = \rho_{xy}(1 - R_0B/\rho_{xy}) = \rho_{xy}\exp(-R_0B/\rho_{xy}). \quad (4)$$

Equation (3) can then be rewritten as

$$\log(\rho_{xy}) - (R_0B/\rho_{xy})\log e = \log(cM) + n\log(\rho_{xx}), \quad (5)$$

or

$$\log(\rho_{xy}) = \log(cM) + 0.4343R_0B/\rho_{xy} + n\log(\rho_{xx}). \quad (6)$$

To extract R_0 from our measurements, we first need to determine the scaling factor n. This can be obtained by plotting $\log(\rho_{xy})$ vs $\log(\rho_{xx})$ measured in high magnetic fields at several low temperatures, where—as noted—both n and cM can be assumed to remain constant. This is shown in Fig. 2(a) for the annealed sample with $y = 0.10$, where the value of n can be obtained from the slope of the straight-line portion of the plot ($T \leqslant 10$ K and $B > 3$ T). Using this value, we then plot the experimental result $\log(\rho_{xy})$–$n\log(\rho_{xx})$ as a function of B for each sample, as shown in Fig. 2(b). Since $\log(\rho_{xy})$–$n\log(\rho_{xx}) = 0.4343(R_0B/\rho_{xy}) + \log(cM)$, we can obtain R_0 from the slope of this plot [note that ρ_{xy} is very nearly constant in the field range used for the plot, as seen in Fig. 1(a)]. From the value of R_0 so obtained, we can now determine the number of itinerant holes in the $Ga_{1-x}Mn_xAs_{1-y}P_y$ film. As for the nonlinearity in Fig. 2(b) seen for low-field data, this arises because the analysis requires full saturation of magnetization, and at lower fields the spins are not entirely aligned. The plots for the remaining five samples are analyzed in the same way (as shown in the Supplemental Material [18]), and the itinerant hole concentrations obtained by this process are tabulated in Table II. As seen in Figs. S1–S6 in the Supplemental Material [18], the low-field departure from linearity increases as the Curie temperature decreases, since there are more randomly oriented spins that need to be aligned, requiring increasingly higher fields for achieving full saturation.
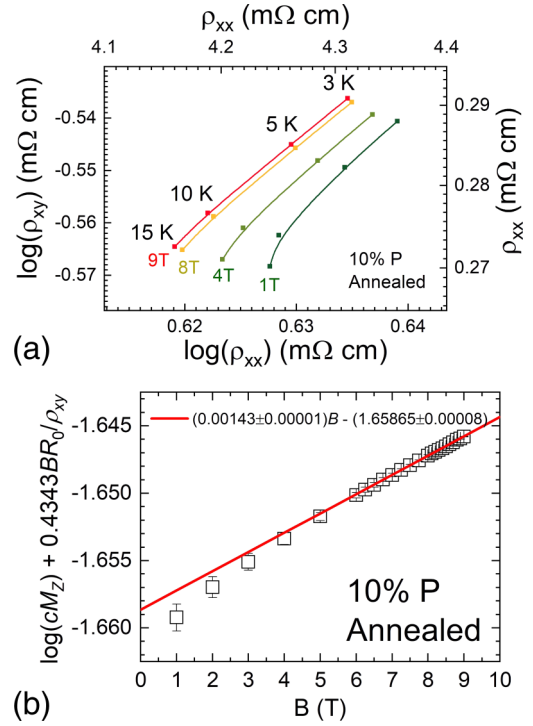

FIG. 2. (a) Logarithmic plot of ρ_{xx} vs ρ_{xy} at several temperatures (3, 5, 10, 15 K) and magnetic fields (1.0–9.0 T) for $Ga_{1-x}Mn_xAs_{1-y}P_y$ with $y = 0.103$. (b) Magnetic field dependence of $\log(cM_z) + 0.4343BR_0/\rho_{xy}$ for the same sample, and linear fit for high-field data.

III. DISCUSSION

A. Hole localization in $Ga_{1-x}Mn_xAs_{1-y}P_y$

In order to discuss the experimental results obtained in this series of measurements, it will be necessary to establish the relationship between the hole concentration and the distribution of Mn in the $Ga_{1-x}Mn_xAs_{1-y}P_y$ lattice. From past work [19] on $Ga_{1-x}Mn_xAs$ we know that during low-temperature MBE growth the majority of Mn enters the $Ga_{1-x}Mn_xAs_{1-y}P_y$ lattice by substitutionally replacing Ga, thus acting as acceptors. We will designate the concentration of this substitutional Mn as x_{sub}. Importantly, a fraction of Mn will also enter the lattice at interstitial positions, and will then act as double donors,

TABLE II. Calculated hole concentrations in $Ga_{0.94}Mn_{0.06}As_{1-y}P_y$ films.

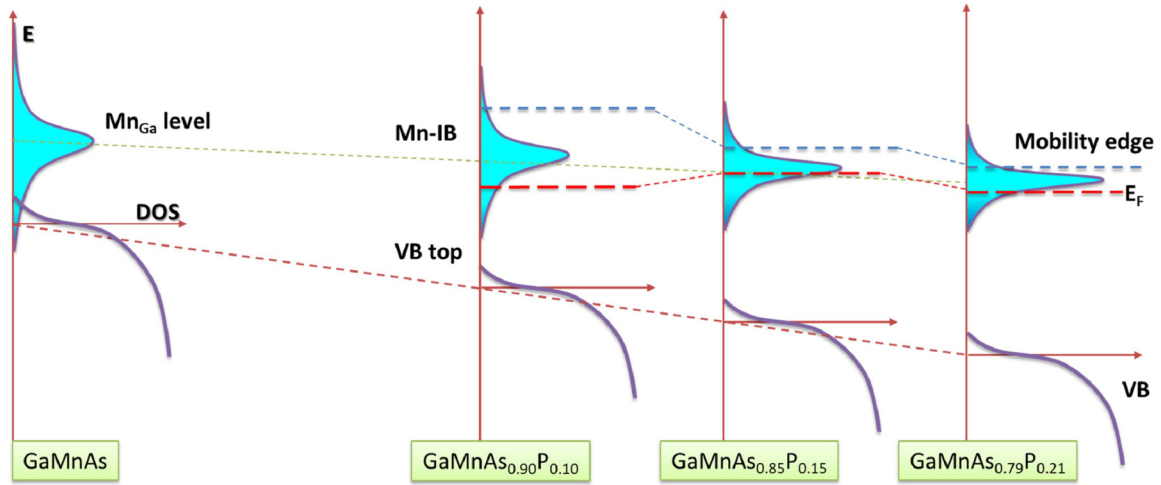| Phosphorus concentration y	0.10	0.15	0.21
Annealed			
x_{sub}	0.051	0.049	0.052
x_i	0.009	0.011	0.008
$p_{tot}(\times 10^{20}\,cm^{-3})$	7.12	6.05	7.99
$P_{deloc}(\times 10^{20}\,cm^{-3})$	6.59	1.84	3.57
As grown			
x_{sub}	0.046	0.045	0.043
x_i	0.014	0.015	0.017
$p_{tot}(\times 10^{20}\,cm^{-3})$	3.78	3.42	1.95
$P_{deloc}(\times 10^{20}\,cm^{-3})$	1.41	0.56	0.38

FIG. 3. Schematic of Mn impurity band (Mn-IB) and the top of the valence band (VB) as a function of phosphorus content. The $Ga_{1-x}Mn_xAs$ diagram is shown for comparison. Note that even though there may be overlap between the valence and impurity bands in the case of $Ga_{1-x}Mn_xAs$, the valence band moves further from the impurity band as phosphorus concentration increases. Note also that the progression of the Fermi level E_F with phosphorus content is not monotonic, since we have attempted to show the larger effect of Mn interstitials in the 15% specimen.

thus compensating the hole concentration in the system. We will designate the concentration of such Mn interstitials as x_i. Finally, a small fraction of Mn will also enter the lattice in the form of Mn precipitates, which have no effect on the electric properties of the alloy except for contributing to its disorder. One should finally note that low-temperature annealing of samples after MBE growth has the effect of transferring a fraction of interstitial Mn into such random Mn precipitates, thus reducing the degree of compensation in the annealed specimens [19,20]. However, it should be recalled that the efficiency of such annealing on eliminating Mn interstitials will also depend on the thickness of the specimen [21], a point that will become important in quantitative discussion of our results later in the manuscript.

It is well established that in GaAs weakly doped with Mn, the Mn acceptor level lies 100.3 meV above the top of the valence band. As the Mn concentration increases to form the $Ga_{1-x}Mn_xAs$ alloy, the acceptor level gradually broadens into an impurity band in which, at sufficiently high Mn concentrations, the holes eventually become delocalized as their wave functions begin to overlap. We note parenthetically that at cryogenic temperatures at which our measurements were carried out, the holes—owing to the relatively large ionization energy of the acceptor level—must be assumed to occupy the impurity band. This will be especially true in $Ga_{1-x}Mn_xAs_{1-y}P_y$ alloys, in which the separation between the valence band and the acceptor impurity band increases progressively with increasing phosphorus concentration. One should note additionally that at large acceptor doping concentrations (as is the case in our alloys) the impurity band itself "pushes" the top of the valence band down, thus increasing that separation even further [22].

We summarize this schematically in Fig. 3. Electrons from the double-donor level arising from the presence of Mn interstitials "fall" into the acceptor band, thus defining the Fermi level. The top of the valence band, and to a lesser degree also the acceptor band, are progressively shifted downward as the

concentration of P increases. The reader will notice that in the figure all bands are drawn with slight extensions at their edges, to account for fluctuation and disorder that is inherent in alloys [23]. Such extensions, and especially the upward extension of the valence band, have been used as grounds for a model in which the top of the valence band is merged with the acceptor band into a single "valence" band. While this picture may be applicable to $Ga_{1-x}Mn_xAs$ because of the proximity of the two bands, it becomes increasingly less appropriate as the separation between the acceptor and valence bands increases with increasing phosphorus concentration, and we will not use it in this paper.

As shown schematically in Fig. 3, the holes reside in the acceptor band, above the Fermi level created by electrons from the compensating donors. However, the mobility of the holes is limited by the topmost part of the impurity band, where they become localized due, primarily, to alloy inhomogeneities and fluctuations in impurity distributions, which form the so-called "mobility edge." Thus the total (i.e., uncompensated) hole concentration must consist of both delocalized holes that are free to move, and holes localized due to the existence of the mobility edge.

In discussing the distribution of Mn ions in the $Ga_{1-x}Mn_xAs_{1-y}P_y$ lattice, we will follow the common practice of using x_{sub} for designating the atomic fraction of Mn substituted at Ga sites (where they act as deep-level acceptors), and x_i for Mn at interstitial sites (where Mn ions act as double donors). Ignoring the very small fraction of random Mn precipitates (since, as already noted, they have negligible effect on electronic properties of the alloy), the total concentration of Mn in the alloy, $x_{tot} = x_{sub} + x_i$, can be obtained from the lattice parameter measured by x-ray diffraction [24,25]. To determine x_{tot} for our set of samples we have used a $Ga_{1-x}Mn_xAs$ film grown at identical MBE conditions as the three $Ga_{1-x}Mn_xAs_{1-y}P_y$ specimens (i.e., the same temperature and Mn flux settings). We recall from the literature that saturation magnetization M_{sat} provides a measure of $x_{eff} =$

$x_{sub}-x_i$ in $Ga_{1-x}Mn_xAs$ by assuming magnetic moment per Mn ion to be $4.5 \mu_B$ [26]. Applying the same approach to our $Ga_{1-x}Mn_xAs_{1-y}P_y$ samples, we obtain x_{eff} from the relation

$$M_{sat} = N_{Mn} 4.5 \mu_B = (4x_{eff}/a^3) 4.5 \mu_B, \qquad (7)$$

where M_{sat} is the value of saturation magnetization listed in Table I for each sample, $N_{Mn} = 4x_{eff}/a^3$ is the net concentration of Mn ions contributing to M_{sat}, and a is the lattice parameter of the alloy obtained from x-ray diffraction, listed in Table I. The values of x_{tot} and x_{eff} obtained in this manner then serve to determine x_{sub} and x_i for each of the samples, as listed in Table II.

It has been shown that, after accounting for compensation by Mn interstitials, the total hole concentration p_{tot} in $Ga_{1-x}Mn_xAs$ is given by [27,28]

$$p_{tot} = 4(x_{sub} - 2x_i)/a^3, \qquad (8)$$

and we will assume that this can also be applied to $Ga_{1-x}Mn_xAs_{1-y}P_y$. In Table II we list the total hole concentration p_{tot} calculated in this way, and the concentration of itinerant (i.e., delocalized) holes p_{deloc} determined by Hall measurements. We note that the values of p_{tot} are consistently larger than p_{deloc} for all samples, thus indicating that in $Ga_{1-x}Mn_xAs_{1-y}P_y$ a large portion of the holes are localized, and thus do not contribute to the Hall effect. This is indicated schematically in Fig. 3, where the highest-energy holes in the impurity band are immobilized above the mobility edge.

Our main objective in this paper is to determine the concentration of delocalized holes in $Ga_{1-x}M_xAs_{1-y}P_y$, and to establish how it is affected by the phosphorus concentration for a constant Mn concentration $x_{tot} = 0.06$. As already noted, we assume that the holes arising from the Mn dopant reside in the impurity band associated with the deep Mn acceptor, indicated in Fig. 3 [29–31]. At Mn concentrations of several atomic percent the net number of acceptors, and thus the number of states in the acceptor impurity band (which is determined by x_{eff} defined above) is sufficiently high for achieving overlap of hole wave functions in the impurity band. Consequently, at these concentrations the holes form extended states and become delocalized. However, band tailing at the upper- and lower-energy limits of the acceptor band results in the formation of mobility edges, resulting in localization of states at those edge energies. As suggested schematically in Fig. 3, the delocalized holes (i.e., holes that contribute to the Hall effect and other transport properties) then correspond to energies between the Fermi level and the mobility edge at the upper region of the acceptor band.

The reader will also see in Table II that the concentrations of delocalized holes measured in annealed samples do not progress monotonically with the concentration of phosphorus y. This is because, in the set of samples available for our measurements, the sample with $y = 0.15$ is considerably thicker than the $y = 0.10$ and $y = 0.21$ specimens. As has already been noted, the effect of annealing depends strongly on sample thickness [21]; i.e., the thinner the sample, the more complete is the removal of Mn interstitials from the material to random Mn clusters, primarily at film surfaces. From this we conclude that in the case of the $y = 0.15$ sample, the removal of Mn interstitials is less complete after annealing

than in the other two specimens, a feature clearly borne out by the calculated values of x_i listed in Table II. As indicated in Fig. 3, the larger value of x_i in that case automatically raises the Fermi level in the acceptor band, thus reducing the number of delocalized holes, in agreement with Hall measurements obtained on the $y = 0.15$ sample after annealing. Direct comparison of the value of p_{deloc} in this sample with p_{deloc} in the annealed $y = 0.10$ and 0.21 specimens is therefore not meaningful. However, the striking contrast in the value of p_{deloc} obtained for the annealed $y = 0.15$ sample compared to the two annealed thinner specimens does serve to underscore how strongly the degree of localization depends on the net concentration of Mn interstitials.

We can, however, meaningfully compare values of hole concentrations in annealed $y = 0.10$ and 0.21 layers, whose thicknesses are nearly the same, and in all as-grown samples, as shown in Table II. From this we immediately note that the value of p_{deloc} decreases (or—equivalently—that the degree of localization rapidly increases) with increasing concentration of phosphorus. We suggest that this increase of localization is directly related to the increasing distance between the acceptor band and the valence band (the greater that distance, the shorter are hole wave functions in the acceptor band). This presence of localization has not been clearly established for $Ga_{1-x}Mn_xAs$ itself, possibly because of greater wave function overlap due to smaller ionization energy of the impurity band (indicated schematically in Fig. 3) in this material. Additionally, it is also possible that the degree of disorder in ternary $Ga_{1-x}Mn_xAs$ is smaller than in the quaternary $Ga_{1-x}M_xAs_{1-y}P_y$, which is expected to reduce the effects of the mobility edge in $Ga_{1-x}Mn_xAs$, thus automatically reducing the degree of localization of the holes.

From past work we also note that in $Ga_{1-x}Mn_xAs$ films the total hole concentration estimated by channeling Rutherford backscattering and particle-induced x-ray emission (*c*-RBS/PIXE) experiments, $p_{tot} = x_{sub}-2x_i$, is in nearly perfect agreement with the hole concentration determined by electrochemical capacitance voltage (ECV) profiling [21,28], thus indicating that the number of mobile holes in $Ga_{1-x}Mn_xAs$ is essentially given by total hole concentration. However, the difference between p_{tot} and p_{deloc} becomes increasingly conspicuous in our series of $Ga_{1-x}M_xAs_{1-y}P_y$ samples as the phosphorus content increases. As has been mentioned earlier, such increase of localization is consistent with the increasing distance between the valence and the acceptor band, which reduces the wave function overlap in the impurity band as the width of the band becomes narrower.

B. Relationship between holes and magnetic properties of $Ga_{1-x}Mn_xAs_{1-y}P_y$

We now inquire into the relationship between the observed concentration of delocalized holes and magnetic properties of the specimens studied in this work. Understanding of ferromagnetic properties of $Ga_{1-x}Mn_xAs$ has been originally developed by assuming that Mn acts as a shallow dopant, producing free holes in the valence band, which then mediate ferromagnetic exchange between Mn ions via the mean-field Ruderman-Kittel-Kasuya-Yosida (RKKY) interaction, assuming a very long Friedel wavelength (i.e., the Zener model)
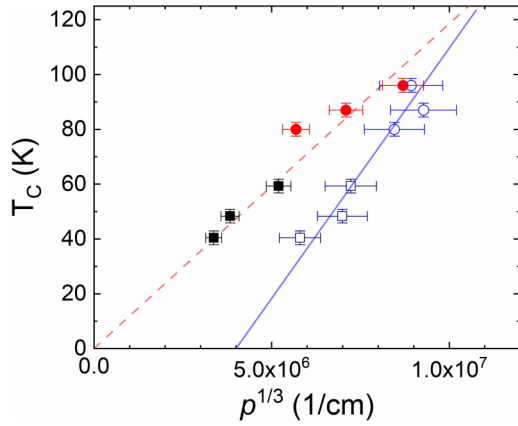
FIG. 4. Red filled circles: Curie temperature T_c as a function of $(p_{\text{deloc}})^{1/3}$ for our three annealed $Ga_{1-x}Mn_xAs_{1-y}P_y$ samples. Black filled squares: Curie temperature T_c as a function of $(p_{\text{deloc}})^{1/3}$ for the same samples before annealing. Open circles: T_C as a function of $(p_{\text{tot}})^{1/3}$ for annealed samples. Open squares: T_C as a function of $(p_{\text{tot}})^{1/3}$ for the same samples before annealing. The dashed line is from T_C vs $p^{1/3}$ as suggested in Ref. [32]. Solid line is a guide for the eye.

[11]. Although the assumption of Mn as a shallow acceptor becomes hard to justify as the valence band and the acceptor band move apart with increasing phosphorus concentration, the Zener model itself can be applied equally well to a system of delocalized holes in the acceptor band itself, as it had originally been to holes in the valence band.

This is illustrated in Fig. 4, in which we plot the Curie temperature T_C as a function of $(p_{\text{deloc}})^{1/3}$. Although we were not able to meaningfully follow the effect of phosphorus content y on p_{deloc} in the three annealed samples because of a significantly larger degree of compensation in the $y = 0.15$ specimen, it is interesting that T_C itself follows the progression of p_{deloc} in the $Ga_{1-x}Mn_xAs_{1-y}P_y$ alloys (both annealed and as grown) as predicted by the Zener model (filled red symbols and filled black symbols), rather than the progression of phosphorus concentration.

In this figure we have also plotted, as open circles and open squares, total concentrations p_{tot} corresponding to the Curie temperatures for our three annealed and three as-grown samples, respectively, calculated using x_{sub} and x_i values in Table II, thus obtaining the relationship between p_{tot} and T_C shown by the solid line. The dashed line in the figure shows the theoretical dependence of T_C as a function of $p^{1/3}$, as suggested by Ref. [32] for the Zener model. It is important to note that the Curie temperatures measured on all samples are in reasonable agreement with the corresponding values of $(p_{\text{deloc}})^{1/3}$, indicating that it is the *delocalized* holes rather than p_{tot} that determine the Curie temperature as shown in Ref. [32].

Two additional insights emerge from the plot of T_C as a function of $(p_{\text{tot}})^{1/3}$ for both the annealed and as-grown

samples (open circle and open square symbols). As seen in the figure, the plot forms an approximately solid blue line, intersecting the x axis at $p^{1/3} \approx 4 \times 10^6 \, \text{cm}^{-1}$, thus indicating that T_C (and therefore ferromagnetism itself) vanishes for concentrations p_{tot} below about $6 \times 10^{19} \, \text{cm}^{-3}$. This indicates a Mott-like metal-insulator transition, as has also been suggested in Refs. [16,33]. In the present context, the observation that the ferromagnetism of $Ga_{1-x}Mn_xAs_{1-y}P_y$ originates when such a minimum concentration of holes is reached strongly supports the assumption that the holes are in the acceptor band, requiring a certain minimum number that is sufficient for wave functions to form an extended continuum, and thus to achieve the hole mobility needed for mediating exchange coupling between the Mn moments in the lattice.

This also indicates that, as the degree of localization increases (as shown by the divergence of the solid and dashed lines in the figure), the Curie temperature decreases, culminating at $T_C = 0$ K when p_{tot} intersects the x axis, thus indicating that at $p_{\text{tot}} = 6 \times 10^{19} \, \text{cm}^{-3}$ all holes are localized, and ferromagnetism of our $Ga_{1-x}Mn_xAs_{1-y}P_y$ alloys vanishes.

IV. CONCLUDING REMARKS

Measurements carried out in this study indicate that there is significant progression of hole localization in $Ga_{1-x}Mn_xAs_{1-y}P_y$ as phosphorus concentration increases in this alloy, as indicated by the degree of divergence of the solid and dashed lines in Fig. 4. Since the number of delocalized holes is limited both by the mobility edge at the upper boundary of the acceptor band and by the acceptor binding energy, we can understand why the number of itinerant states is reduced in the system as the phosphorus content increases. Importantly, this analysis highlights the impact of localization on magnetic properties of $III_{1-x}Mn_xV$ semiconductors generally. While such effects have been previously studied in $Ga_{1-x}Mn_xAs$ [34], they have remained challenging to understand. Our work shows that $Ga_{1-x}Mn_xAs_{1-y}P_y$ allows us to reliably tailor and quantify localization near impurity band edges that are well separated from the valence band. The introduction of both Mn and P thus points to an unprecedented correlation between localization and the suppression of magnetism in $Ga_{1-x}Mn_xAs_{1-y}P_y$.

While the results of this study shed important light on the behavior of the $Ga_{1-x}Mn_xAs_{1-y}P_y$ alloy, they also open a number of significant questions that will require further investigation. In particular, they enable the characterization of a parameter space in the phase diagram of the $III_{1-x}Mn_xV_{1-y}$ systems near the possible metal-insulator transition, that accompanies the emergence of magnetic order.

[1] A. Lemaître, A. Miard, L. Travers, O. Mauguin, L. Largeau, C. Gourdon, V. Jeudy, M. Tran, and J.-M. George, Strain control of the magnetic anisotropy in (Ga,Mn) (As,P) ferromagnetic semiconductor layers, Appl. Phys. Lett. **93**, 021123 (2008).

[2] A. W. Rushforth, M. Wang, N. R. S. Farley, R. P. Campion, K. W. Edmonds, C. R. Staddon, C. T. Foxon, and B. L. Gallagher, Molecular beam epitaxy grown (Ga,Mn)(As,P) with perpendicular to plane magnetic easy axis, J. Appl. Phys. **104**, 073908 (2008).

[3] M. Cubukcu, H. J. von Bardeleben, K. Khazen, J. L. Cantin, O. Mauguin, L. Largeau, and A. Lemaître, Adjustable anisotropy in ferromagnetic (Ga,Mn) (As,P) layered alloys, Phys. Rev. B **81**, 041202(R) (2010).

[4] H. Lee, J. Chang, P. Chongthanaphisut, S. Lee, S. Choi, S.-K. Bac, A. R. Nasir, S. Lee, A. Pardo, S. Dong, X. Li, X. Liu, J. K. Furdyna, and M. Dobrowolska, Magnetic anisotropy of quaternary GaMnAsP ferromagnetic semiconductor, AIP Adv. **7**, 055809 (2017).

[5] X. Li, X. Liu, S. Dong, C. Gorsak, J. K. Furdyna, M. Dobrowolska, S.-K. Bac, S. Lee, and S. Rouvimov, Dependence of ferromagnetic properties on phosphorus concentration in $Ga_{1-x}Mn_xAs_{1-y}P_y$, J. Vac. Sci. Technol. B **36**, 02D104 (2018).

[6] V. K. Vlasko-Vlasov, W.-K. Kwok, S. Dong, X. Liu, M. Dobrowolska, and J. K. Furdyna, Extreme asymmetry of Néel domain walls in multilayered films of the dilute magnetic semiconductor (Ga,Mn)(As,P), Phys. Rev. B **98**, 180411(R) (2018).

[7] R. F. Need, S.-K. Bac, X. Liu, S. Lee, B. J. Kirby, M. Dobrowolska, J. Kossut, and J. K. Furdyna, Magnetic properties and electronic origin of the interface between dilute magnetic semiconductors with orthogonal magnetic anisotropy, Phys. Rev. Mater. **4**, 054410 (2020).

[8] T. Niazi, M. Cormier, D. Lucot, L. Largeau, V. Jeudy, J. Cibert, and A. Lemaître, Electric-field control of the magnetic anisotropy in an ultrathin (Ga,Mn)As/(Ga,Mn)(As,P) bilayer, Appl. Phys. Lett. **102**, 122403 (2013).

[9] E. De Ranieri, P. E. Roy, D. Fang, E. K. Vehsthedt, A. C. Irvine, D. Heiss, A. Casiraghi, R. P. Campion, B. L. Gallagher, T. Jungwirth, and J. Wunderlich, Piezoelectric control of the mobility of a domain wall driven by adiabatic and non-adiabatic torques, Nat. Mater. **12**, 808 (2013).

[10] S. Dong, Y.-L. Wang, S.-K. Bac, X. Liu, V. Vlasko-Vlasov, W.-K. Kwok, S. Rouvimov, S. Lee, M. Dobrowolska, and J. K. Furdyna, Programmable bias field observed in graded ferromagnetic semiconductor films with broken symmetry, Phys. Rev. Mater. **3**, 074407 (2019).

[11] T. Dietl, H. Ohno, F. Matsukura, J. Cibert, and D. Ferrand, Zener model description of ferromagnetism in zinc-blende magnetic semiconductors, Science **287**, 1019 (2000).

[12] M. Yahyaoui, H. Riahi, M. A. Maaref, K. Boujdaria, A. Lemaître, L. Thevenard, and C. Gourdon, Magneto-optical Kerr spectroscopy of (Ga,Mn)(As,P) ferromagnetic layers: Experiments and $k \cdot p$ theory, J. Appl. Phys. **121**, 125702 (2017).

[13] W. Ouerghui, H. B. Abdallah, and K. B. Saad, First-principles calculations on magnetism and exchange interactions in GaMnAs and GaMnAsP, Phys. Status Solidi B **254**, 1700115 (2017).

[14] N. Tesařová, D. Butkovičová, R. P. Campion, A. W. Rushforth, K. W. Edmonds, P. Wadley, B. L. Gallagher, E. Schmoranzerová, F. Trojánek, P. Malý, P. Motloch, V. Novák, T. Jungwirth, and P. Němec, Comparison of micromagnetic parameters of the ferromagnetic semiconductors (Ga,Mn)(As,P) and (Ga,Mn)As, Phys. Rev. B **90**, 155203 (2014).

[15] M. Cubukcu, H. J. von Bardeleben, J. L. Cantin, I. Vickridge, and A. Lemaitre, Ferromagnetism in $Ga_{0.90}Mn_{0.10}As_{1-y}P_y$:

From the metallic to the impurity band conduction regime, Thin Solid Films **519**, 8212 (2011).

[16] S. Shen, X. Liu, Z. Ge, J. K. Furdyna, M. Dobrowolska, and J. Jaroszynski, Scaling of the anomalous Hall effect in low Mn concentration (Ga,Mn)As, J. Appl. Phys. **103**, 07D134 (2008).

[17] S. Onoda, N. Sugimoto, and N. Nagaosa, Quantum transport theory of anomalous electric, thermoelectric, and thermal Hall effects in ferromagnets, Phys. Rev. B **77**, 165103 (2008).

[18] See Supplemental Material at http://link.aps.org/supplemental/10.1103/PhysRevMaterials.5.014402 for the data plots of all six samples, and the data and error analysis.

[19] K. M. Yu, W. Walukiewicz, T. Wojtowicz, I. Kuryliszyn, X. Liu, Y. Sasaki, and J. K. Furdyna, Effect of the location of Mn sites in ferromagnetic $Ga_{1-x}Mn_xAs$ on its Curie temperature, Phys. Rev. B **65**, 201303(R) (2002).

[20] I. Kuryliszyn-Kudelska, J. Z. Domagala, T. Wojtowicz, X. Liu, E. Lusakowska, W. Dobrowolski, and J. K. Furdyna, Effect of Mn interstitials on the lattice parameter of $Ga_{1-x}Mn_xAs$, J. Appl. Phys. **95**, 603 (2004).

[21] K. M. Yu, W. Walukiewicz, T. Wojtowicz, J. Denlinger, M. A. Scarpulla, X. Liu, and J. K. Furdyna, Effect of film thickness on the incorporation of Mn interstitials in $Ga_{1-x}Mn_xAs$, Appl. Phys. Lett. **86**, 042102 (2005).

[22] A. M. Cook and M. Berciu, Evolution of the impurity band in a weakly doped, highly compensated semiconductor, Phys. Rev. B **85**, 235130 (2012).

[23] P. Van Mieghem, Theory of band tails in heavily doped semiconductors, Rev. Mod. Phys. **64**, 755 (1992).

[24] J. Sadowski, R. Mathieu, P. Svedlindh, J. Z. Domagała, J. Bak-Misiuk, K. Światek, M. Karlsteen, J. Kanski, L. Ilver, H. Åsklund, and U. Södervall, Structural and magnetic properties of GaMnAs layers with high Mn-content grown by migration-enhanced epitaxy on GaAs(100) substrates, Appl. Phys. Lett. **78**, 3271 (2001).

[25] J. Mašek, J. Kudrnovský, and F. Máca, Lattice constant in diluted magnetic semiconductors (Ga,Mn)As, Phys. Rev. B **67**, 153203 (2003).

[26] T. Jungwirth, J. Sinova, J. Mašek, J. Kučera, and A. H. MacDonald, Theory of ferromagnetic (III,Mn)V semiconductors, Rev. Mod. Phys. **78**, 809 (2006).

[27] K. M. Yu, W. Walukiewicz, T. Wojtowicz, W. L. Lim, X. Liu, Y. Sasaki, M. Dobrowolska, and J. K. Furdyna, Determination of free hole concentration in ferromagnetic $Ga_{1-x}Mn_xAs$ using electrochemical capacitance-voltage profiling, Appl. Phys. Lett. **81**, 844 (2002).

[28] T. Wojtowicz, J. K. Furdyna, X. Liu, K. M. Yu, and W. Walukiewic, Electronic effects determining the formation of ferromagnetic $III_{1-x}Mn_xV$ alloys during epitaxial growth, Phys. E (Amsterdam, Neth.) **25**, 171 (2004).

[29] K. S. Burch, D. B. Shrekenhamer, E. J. Singley, J. Stephens, B. L. Sheu, R. K. Kawakami, P. Schiffer, N. Samarth, D. D. Awschalom, and D. N. Basov, Impurity Band Conduction in a High Temperature Ferromagnetic Semiconductor, Phys. Rev. Lett. **97**, 087208 (2006).

[30] M. Dobrowolska, K. Tivakornsasithorn, X. Liu, J. K. Furdyna, M. Berciu, K. M. Yu, and W. Walukiewicz, Controlling the Curie temperature in (Ga,Mn)As through location of the Fermi level within the impurity band, Nat. Mater. **11**, 444 (2012).

[31] M. Tanaka, S. Ohya, and P. N. Hai, Recent progress in III-V based ferromagnetic semiconductors: Band structure, Fermi

level, and tunneling transport, Appl. Phys. Rev. **1**, 011102 (2014).

[32] A. H. MacDonald, P. Schiffer, and N. Samarth, Ferromagnetic semiconductors: Moving beyond (Ga,Mn)As, Nat. Mater. **4**, 195 (2005).

[33] X. Liu, S. Shen, Z. Ge, W. L. Lim, M. Dobrowolska, J. K. Furdyna, and S. Lee, Scaling relations between anomalous Hall and longitudinal transport coefficients in metallic (Ga,Mn)As films, Phys. Rev. B **83**, 144421 (2011).

[34] A. Richardella, P. Roushan, S. Mack, B. Zhou, D. A. Huse, D. D. Awschalom, and A. Yazdani, Visualizing critical correlations near the metal-insulator transition in $Ga_{1-x}Mn_xAs$, Science **327**, 665 (2010).